Available online at www.sciencedirect.com
ScienceDirect
Journal of the European Ceramic Society 27 (2007) 3425–3431
www.elsevier.com/locate/jeurceramsoc

Effect of interface roughness and coating thickness on interfacial shear mechanical properties of EB-PVD yttria-partially stabilized zirconia thermal barrier coating systems

Shuqi Guo [a,*], Yoshihisa Tanaka [a], Yutaka Kagawa [a,b]

[a] *Composites and Coatings Center, National Institute for Materials Science, 1-2-1 Sengen, Tsukuba, Ibaraki 305-0047, Japan*
[b] *Research Center for Advanced Science and Technology, The University of Tokyo, 4-6-1 Komaba, Meguro-ku, Tokyo 153-8505, Japan*

Received 8 October 2006; received in revised form 1 February 2007; accepted 10 February 2007
Available online 29 March 2007

Abstract

The effect of interface roughness and thickness of thermal barrier coating (TBC) on the interfacial shear mechanical properties of electron beam-physical vapor deposited (EB-PVD)-TBC was examined using as-sprayed and polished bond coats (BC) 200 μm and 500 μm TBC thickness systems, by using a barb test method. The residual compressive stress in the TBC layer from the interface to the top surface was measured, by using Raman spectroscopy. The interface toughness related to the interface roughness and the thickness of the TBC. The interface toughness was larger for the BC as-sprayed TBC system than for the BC polished TBC system. The delamination of the TBC propagated within the TBC layer adjacent to the interface for the BC as-sprayed TBC; for the BC polished TBC, this occurred at the interface between the TGO and the BC. Moreover, the interface toughness was larger in the 500 μm thickness TBC than in the 200 μm thickness TBC. The relation of interface toughness to interface roughness and thickness of the TBC was associated with the interface residual compressive stress and with the interface sliding friction during the delamination of TBC.

Keywords: ZrO_2; Thermal barrier coating; Mechanical properties; Interfaces

1. Introduction

Thermal barrier coatings (TBCs) are enabling materials in the design of advanced gas turbine engine systems.[1,2] Based on ceramics with low thermal conductivity, such coatings provide thermal insulation to actively cooled metallic components, allowing designers to optimize system performance by maximizing combustion temperatures. Given the role of TBCs in shielding structural components from damaging thermal environments, coating durability is of primary importance. Among the TBCs, air plasma-sprayed (APS) and electron beam physical vapor deposited (EB-PVD) yttria-partially stabilized zirconia TBCs have been widely studied in recent years because of their potential ability to substantially extend turbine lives and improve engine efficiencies.[1–5] In particular, EB-PVD-TBCs have recently received attention because the coatings are expected to surpass APS-TBCs in mechanical performance, owing to their specific columnar structure. Thus, understanding the mechanisms that dictate coating failure of the EB-PVD-TBCs has been the subject of intense research.

It is well-known that coating failure is governed by a series of events that include crack nucleation, propagation and coalescence, leading to coating spallation.[5–11] For failures caused by the large compressive stresses that develop within the coating, delamination crack growth occurs under principally mode II loading—particularly for longer cracks with fully developed crack wake contact zones. Hence, the durability or lifetime is a direct function of the mode II toughness of the interface. Thus, it is important for understanding failure behavior of TBC to measure interface fracture toughness between the TBC and bond coat. The authors[12] have recently reported a novel methodology, the barb test method, for measuring the interfacial fracture toughness of the TBC systems. The approach is particularly useful in capturing crack growth behavior under mode II loading conditions, and is amenable to measurement of both short-crack

* Corresponding author. Tel.: +81 29 859 2223; fax: +81 29 859 2401.
E-mail address: GUO.Shuqi@nims.go.jp (S. Guo).

0955-2219/$ – see front matter © 2007 Elsevier Ltd. All rights reserved.
doi:10.1016/j.jeurceramsoc.2007.02.196

and long-crack behavior. The authors successfully measured the interface toughness of an EB-PVD-TBC system, through using this technique. However, the influences of the interface roughness and the thickness of the TBC on the interface toughness are little known. Therefore, it is required for the EB-PVD-TBC systems to learn the effect of interface roughness and coating thickness on the interfacial shear mechanical properties. In this work, the interface toughness of EB-PVD-TBC was measured in three TBC systems with different interface roughness and coating thickness, by using a barb test method. The effects of interface roughness and coating thickness on the interface toughness were examined.

2. Experimental

2.1. Materials

The materials used in this study were prepared by the electron beam physical vapor depositing (EB-PVD) of 4 mol% Y_2O_3-partially stabilized ZrO_2 powder on a MA738LC nickel-based superalloy substrate with a NiCoCrAlY bond coat overlayer. The bond coat (BC) was deposited by low-pressure plasma spray deposition to a thickness of ∼100 μm, and has an overall composition of 32 wt.% Ni, 21 wt.% Cr, 8 wt.% Al, 0.5 wt.% Y, with the balance Co. The deposition of TBC was performed on a high-powder EB-PVD coater (Von Ardenne Anlagentechnik GmbH/TUBA150) directly on the substrate plates. This coater consists of three chambers: loading chamber, heating chamber and coating chamber. Before the substrates were loaded onto a rotation stage in an electron beam deposition chamber, the BC surfaces were polished up to 800 grit and cleaned using an ultrasonic cleaner. The substrates were preheated up to 950 °C by a graphite heater in the heating chamber for ∼20 min below a vacuum prior to deposition. The preheated substrates were then transferred to the coating chamber that was heated to approximately 800 °C. The TBC layers of 200 μm and 500 μm thickness were respectively deposited on the substrates kept at 950 °C with an electron-beam power of 45 kW, a chamber pressure of 1.0 Pa, and a stage rotation speed of 5 rpm. During deposition, oxygen is passed through the coating chamber, in turn this results in the formation of a thermally growth oxide (TGO) layer between the TBC layer and the BC. In addition, in order to obtain a rough interface, a TBC layer of 500 μm thickness was deposited on an "as-sprayed" BC substrate under the same process condition. These EB-PVD-TBC systems were supplied by the JFCC (Japan Fine Ceramics Center, Nagoya, Japan). The obtained three kinds of TBC systems were therefore:

(1) PL-TBC200: BC polished with 200 μm TBC thickness;
(2) PL-TBC500, BC polished with 500 μm TBC thickness;
(3) AS-TBC500, BC "as-sprayed" with 500 μm TBC thickness.

After deposition, the cross-section of the TBC was polished with a diamond paste with granules of down to 1 μm in size. The interface morphology between the TBC and the BC was characterized by scanning electron microscopy (SEM).

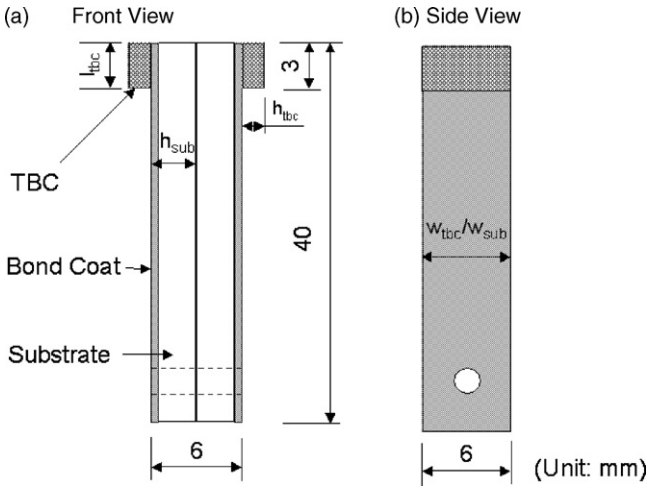

Fig. 1. Shape and dimensions of the specimen for barb testing.

2.2. Interfacial shear mechanical properties measurement

Test specimens with dimensions of 40 mm × 6 mm × 3 mm were cut from the EB-PVD-processed TBC specimens, using a conventional mechanical cutting procedure. The cut faces were ground through standard metallurgical procedures to (1) obtain specimens with the desired final thickness, (2) introduce parallel surfaces, and (3) eliminate mechanical flaws introduced during the cutting process. The TBC layers were then notched at a distance of 3 mm from the end of the specimens, to define the length over which crack growth occurs. The remaining TBC segments were carefully removed with a WC polishing tool. Two specimen pieces prepared in this manner were then affixed back-to-back, using an alignment tool and epoxy adhesive, to form the final barb test specimens. The shape and dimensions of the obtained barb test specimen are shown in Fig. 1.

The barb tests were performed in ambient air at room temperature using a screw-driven mechanical test system (Model Autograph AG-500E, Shimadzu Corp., Kyoto, Japan). The schematic illustration of the loading fixture utilized for the barb testing is shown in Fig. 2. Details of test fixture for barb test method were reported elsewhere.[12] Testing was performed with a constant crosshead displacement rate of 0.1 mm/min. The force-displacement response during the barb testing was digitized and continuously recorded using a digital memory scope (ORM 1200, Yokogawa Electric, Tokyo, Japan). A minimum of five specimens were tested for each measurement. After test completion, the specimens were examined using SEM to investigate the crack path selection, and general morphology of the fracture surfaces. In addition, the fracture surface after the testing was analyzed using a Laser meter (1LM15, Laser Tech Co., Tokyo, Japan) to determine the interface roughness.

2.3. Measurement of residual stress

The biaxial stress in the TBC layer was measured by Raman spectroscopy for the TBC coatings at various states, in a manner was similar to that reported elsewhere.[13,14] The measurements have been conducted at room temperature in ambient air using

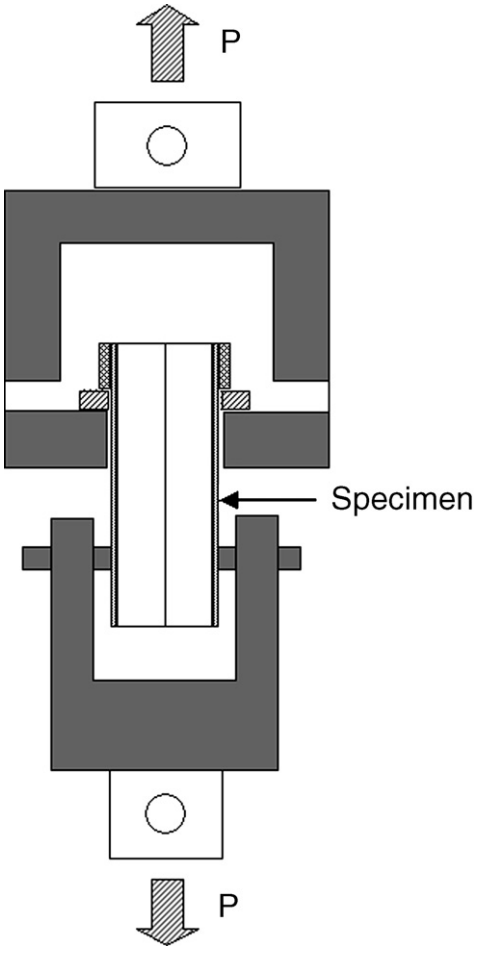

Fig. 2. Schematic illustration of the loading fixture utilized for the barb testing.

a green laser at wavelength of 532 nm in a specially designed micro-Raman spectrophotometer (NRS-1000, Special version, JASCO Co., Tokyo, Japan) to obtain the Raman shift for the TBC. A laser spot (with a size of 4 μm) was positioned and scanned in the TBC layer along the TBC/TGO interface as well as from the interface to the top surface at intervals of 20 μm. In the present study, the shift for the tetragonal ZrO_2 Raman line located at about 640 cm^{-1} was used to calculate the residual stresses in the TBC layer. Details of the procedure were reported elsewhere.[13] In addition, in order to calculate the residual stress, a previous calibration was required[15] and for the TBC studied each cm^{-1} of shift corresponds to 220 MPa. Thus, the biaxial stress in the TBC can be given according to the relationship between the frequency shift and the biaxial stress as in the following:

$$\sigma = 0.22(\Pi_0 - \Pi_i) \quad (1)$$

where σ is the biaxial stress (GPa), Π_0 the Raman shift from the Raman peak at the stress-free condition which is to be 640 cm^{-1}, and Π_i is the Raman shift from the Raman peak at a stressed condition.

3. Results

3.1. Interface morphology

In Fig. 3, SEM micrographs of the interface morphology between the TBC and the BC for the studied TBC systems are presented. A thin thermally grown oxide (TGO) layer is shown in darker contrast between the TBC and the BC. The formation of the TGO layer is a result of the inward diffusion of oxygen and the outward diffusion of Al during the deposition.

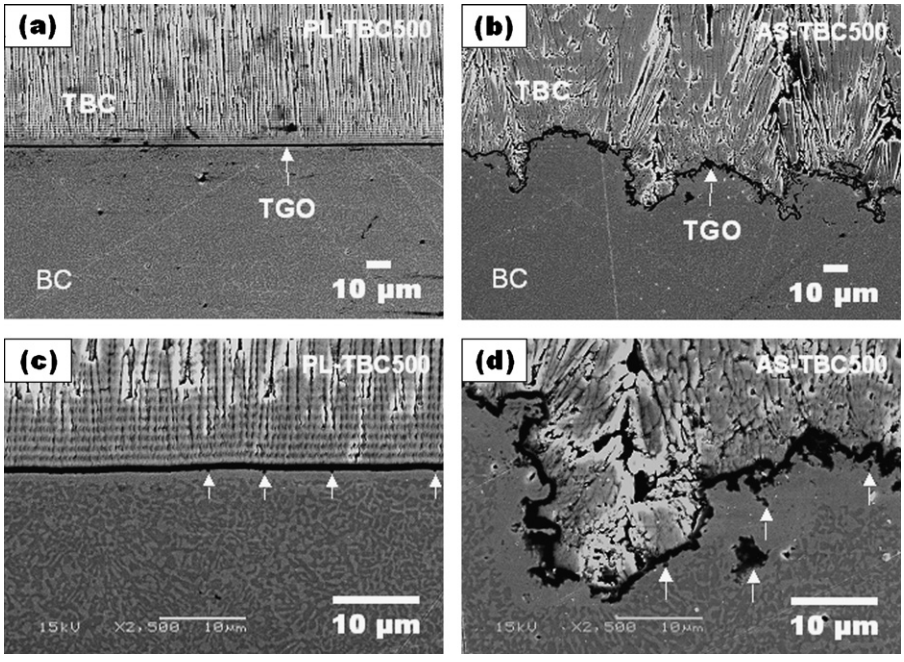

Fig. 3. Typical SEM images of interface morphology between the TBC and the BC in the EB-PVD-TBC systems: (a and c) PL-TBC500, and (b and d) AS-TBC500, showing a rough interface for AS-TBC500 compared with PL-TBC500.

For PL-TBC200 and PL-TBC500, the low-magnification image reveals that the TGO layer is relatively flat (Fig. 3(a)), and its thickness is approximately 0.5 and 0.8 μm, respectively. Under high-magnification image (Fig. 3(c)), although the TGO layer is smooth at the TBC side, at the BC side certain 'blocky' particles 0.2–0.7 μm in diameter are present (indicated by arrows in Fig. 3(c)). This indicated that the TGO protruded into the BC in some locations. Differing from the PL-TBC200 and PL-TBC500, for the AS-TBC500 the interface reveals a sawtoothed shape (Fig. 3(b)), showing the undulated nature of the BC/TGO interface. The TGO layer is not uniform between the TBC and the BC, and its thickness has a range of 0.5–2 μm. High-magnification image reveals details of the TGO, TBC and BC near the interface (Fig. 3(d)). Block particles 1–3 μm in diameter are formed at the TGO front adjacent to the BC. In isolated locations, the TGO appears to form within the BC beneath the interface (indicated by arrows in Fig. 3(d)).

3.2. Interface mechanical properties

3.2.1. Force–displacement curve

In Fig. 4, typical plots of response load versus crosshead displacement (P–u), obtained from barb testing of the studied EB-PVD-TBC systems are presented. These curves show a similar response of load to displacement. The load increases nearly linearly up to a load, P_d, at which a small load drop happened, with the exception of an initial nonlinear segment corresponding to compliance associated with test fixture and specimen alignment in the self-aligning mechanisms. The load, P_d, corresponds to the point at which the applied load is sufficient to initiate delamination of the TBC layer from the underlying substrate. After the initial load drops, the load increases to the maximum load, and then the load dropped sharply. In particular, in the case of PL-TBC200, the load dropped for three or four times prior to complete delamination. This behavior suggests that the propagation of the interfacial delamination occurs incrementally. Complete decohesion coincides with the final drop to zero response force.

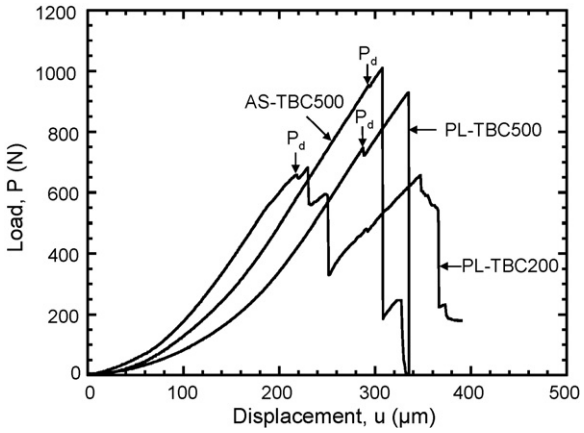

Fig. 4. Typical force–displacement curves obtained during the barb testing for the three studied EB-PVD-TBC systems.

3.2.2. Fracture surface observations

In Fig. 5, typical SEM micrographs of the exposed metallic BC side of the fracture surface after TBC delamination for the studied TBC systems are presented. In the case of PL-TBC500, the low-magnification image reveals the complex crack growth behavior under shear loading mode. The failure surface was a mixture of exposed metallic BC, regions of TGO, and remaining thin TBC layer (Fig. 5(a)). In addition, some wear tracks were observed on the exposed fracture surface. High-resolution image showed more clearly the fractured, embedded segments

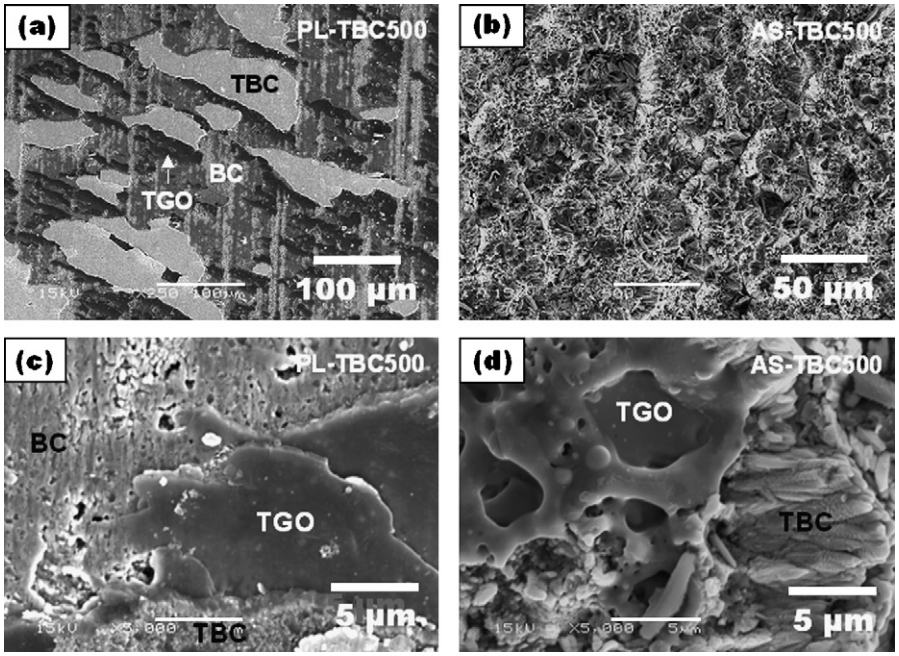

Fig. 5. SEM images of the fracture surfaces on the metallic substrate side exposed by the delamination of the TBC layer in the EB-PVD-TBC systems: (a and c) PL-TBC500, and (b and d) AS-TBC500 (TBC: thermal barrier coating, BC: bond coat, and TGO: thermally growth oxide).

of TGO and the thin TBC layer bonded to these TGO particles (Fig. 5(c)). This indicated that the delamination occurs along a mixed pathway through TGO/BC or TBC/TGO interfaces. This interface delamination behavior is independent of the thickness of TBC.

In the case of AS-TBC500, on the other hand, the low-magnification image shows that the fracture surface on the metallic BC site was relatively rough compared with PL-TBC500 (Fig. 5(a and b)). Under high-magnification SEM examinations, it is clearly revealed that the fracture surface is principally TBC with some patches of TGO (Fig. 5(d)). Also, columnar grains consisting of TBC may be observed. This indicated that the delamination proceeded essentially within the TBC layer, with the crack propagating along either the TGO/TBC interface or the TBC layer adjacent to the TGO layer, as a result of the presence of pores and cracks within the TBC layer adjacent to the TGO which provide a cracking source for the EB-PVD-TBC system studied. This difference in crack propagation path for the two TBC systems is attributable to the BC surface roughness before deposition that controlled the properties of the TBC layer formed near the interface.

3.2.3. Interfacial toughness

Assuming (1) that all of the strain energy stored in the TBC layer and the substrate prior to initiating delamination is released in developing new surface area during crack propagation, and (2) that the delamination is uniform along the crack tip without buckling, the interfacial toughness, G_i, for a TBC system is approximately obtained[12] from barb test by

$$G_i \approx \frac{P_d^2}{4}\left(\frac{1}{E_{sub}h_{sub}w_{sub}^2}+\frac{1}{E_{tbc}h_{tbc}w_{tbc}^2}\right) \quad (2)$$

where E, h and w are Young's modulus, thickness and width of specimen, respectively, the subscripts sub and tbc refer to the substrate and the TBC layer, respectively. For the test configuration used here (Fig. 1), the thickness of the substrate, h_{sub}, is much greater than that of the TBC layer, h_{tbc} ($h_{sub} \gg h_{tbc}$), and the width of the substrate and the TBC is the same, i.e., $w_{sub} = w_{tbc}$. Young's modulus is taken to be $E_{sub} = 200$ GPa for the substrate[16] and $E_{tbc} = 44$ GPa for the EB-PVD-TBC.[17] Here, the anisotropic nature of the TBC elastic properties is neglected. Because the initial load drop obtained in the P–u curve is believed to correspond to the onset of the TBC layer delamination from the substrate, the interface toughness of the TBC layer from the substrate is determined using equation (2) with the initial force, P_d; the instantaneous force drop behavior after the maximum load (Fig. 4) was neglected. It is found that the measured average interface toughness was approximately 84 J/m^2 and 106 J/m^2 for the PL-TBC200 and PL-TBC500, respectively. In the case of AS-TBC500, the obtained interface fracture toughness was approximately 123 J/m^2. With the present experimental method, these values are roughly the mode II strain energy release rates ($\psi \approx 90^\circ$) for either the TBC/BC interface or the TBC layer, dependent upon the observed fracture path selection.

3.3. Residual stress

The interface residual compressive stress measured along the TBC/TGO interface is summarized in Table 1. The interface compressive residual stress is larger for PL-TBC500 than for PL-TBC200, showing that the thick TBC layer led to larger interface residual compressive stress. In addition, it is found that the interface residual compressive stress is larger for PL-TBC500 than for AS-TBC500. It is known that the interface residual compressive stress is caused by the growth strains in TGO and the thermal expansion misfit between the TGO and the TBC. Thus, it is believed that the major cause of low residual compressive stress for AS-TBC500 is the presence of defects (pores and cracks, Fig. 3) in the TBC layer adjacent to the interface because these defects result in a relaxation of the interface residual compressive stress.

In Fig. 6, an example of the distributions of the residual compressive stress in the TBC layer from the interface to the top surface for the studied TBC systems is presented. In the case of PL-TBC200 and PL-TBC500, the residual compressive stress

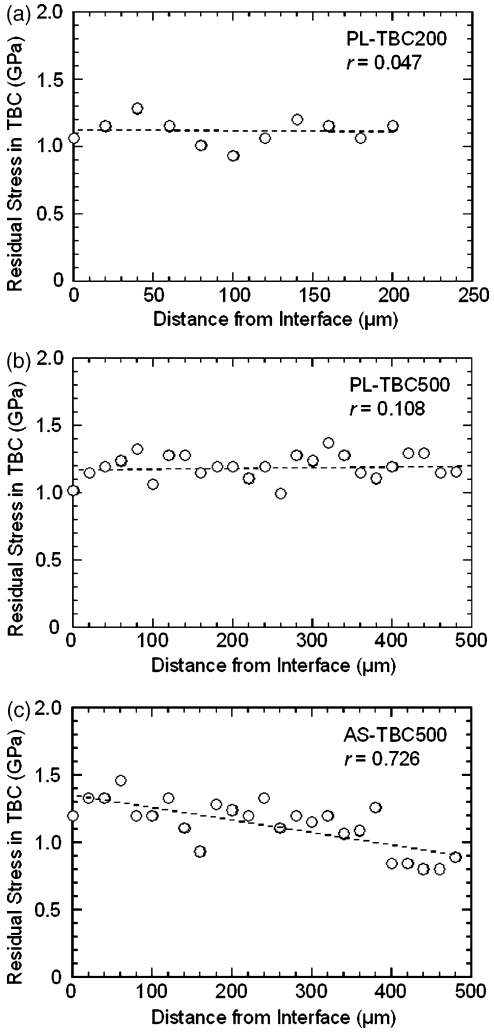

Fig. 6. Distributions of residual compressive stress in the TBC layer from the interface to the top surface for (a) PL-TBC200, (b) PL-TBC500, and (c) AS-TBC500.

Table 1
Average interface compressive residual stress, average interface roughness amplitude, and average interface toughness

Coating materials	Average interface residual stress, σ_r (GPa)	Average interface roughness amplitude, A_r (μm)	Interface fracture toughness, G_i (J/m^2)
PL-TBC200	0.934	15.15	84
PL-TBC500	1.284	16.20	106
AS-TBC500	1.216	22.95	123

in the TBC layer showed almost no change from the interface to the top surface, independent of the thickness of the TBC, i.e., no significant relation between the residual compressive stress and the measurement position in the TBC layer ($r = 0.047$ and 0.108). On the contrary, in the case of AS-TBC500, the residual compressive stress in the TBC layer significantly decreased from the interface to the top surface, showing significant relation of the residual compressive stress to measurement position ($r = 0.726$). This larger difference in the distribution of the residual compressive stress for BC as-sprayed and polished TBC is presumably to be attributed to a stronger ratcheting of the TGO with the TBC for AS-TBC500 than for PL-TBC200 and PL-TBC500, as a result of the smooth interface between the TBC and the BC for the latter compared with the former (Fig. 3). This stronger ratcheting at the interface for AS-TBC500 led to the residual compressive stress slope from the interface to the top surface on cooling because the thermal expansion coefficient of the BC material is larger than that of the TBC material.

4. Discussion

It is known that the interface toughness is linked to the properties of the BC, TGO, and TBC as well as to the interface roughness and thickness of TBC. In the studied TBC system, the interface roughness and thickness of the TBC affect the residual compressive stress at the interface and in the TBC layer, in turn affecting the delamination crack propagation path as well as the interface toughness. In Fig. 7, a correlation of the interface toughness to the residual compressive stress at the interface for the studied TBC systems is presented. It is found that the interface toughness of AS-TBC500 is the largest among the three studied TBC systems although the residual compressive stress at the interface is lower for AS-TBC500 than for PL-TBC500 (Table 1). This finding suggested that the rough interface led to larger interface toughness because of the presence of a sawtoothed shape interface for AS-TBC500 compared with a flat interface for PL-TBC500 (Fig. 3). The roughness of fracture surfaces after delamination for the studied TBC systems was measured under a laser optical microscopy; the observed images are shown in Fig. 8. This clearly shows that the interface roughness is larger for AS-TBC500 than for PL-TBC500. This is consistent with SEM observations of post-tested specimens (Fig. 5). The measured average roughness amplitude of the interface for three studied TBC systems is shown in Table 1. It is seen that the average roughness amplitude is significantly larger for AS-TBC500 than for PL-TBC200 and PL-TBC500. This suggests that a possible reason for the high interface toughness obtained in AS-TBC500 is correlated with interface frictional contribution between the TBC and the BC evidenced by the presence of significant wear tracks observed in the SEM views of

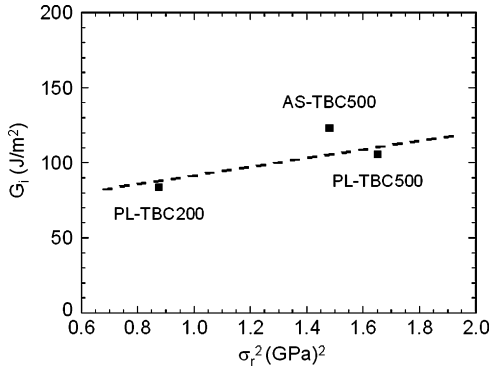

Fig. 7. Plot of interface toughness as a function of average interfacial residual compressive stress.

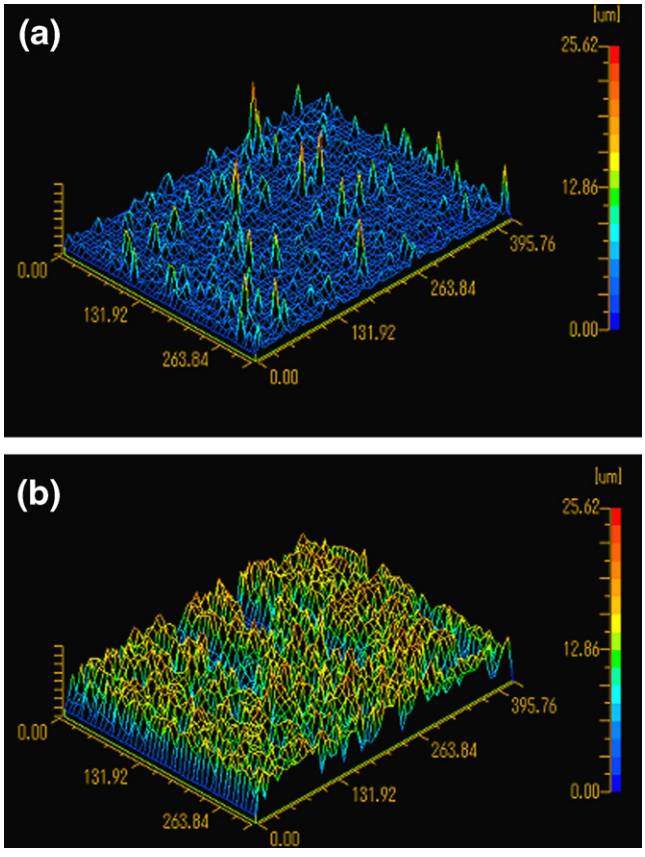

Fig. 8. Examples of interface roughness measured on fracture surfaces for the EB-PVD-TBC systems: (a) PL-TBC500, and (b) AS-TBC500.

the post-tested specimens (Fig. 5(a)). The wear tracks observed on the failure surfaces show that the crack faces remained in contact during crack advance because the presence of the wear tracks indicated a sliding along the spalling interface during the testing. The influence of interface friction on the interface toughness is documented in the literature. Mumm and Evans[18] showed that the mode II toughness value of the TGO/BC interface ($\Gamma_{II} \approx 56\,J/m^2$)[18] was lower than that of the oxide ($\Gamma_{II} \geq 100\,J/m^2$).[19] This low mode II toughness is attributable to the bending effect of the TGO/TBC bilayer as well as to shortening of the zone subject to friction over the full length of the delamination. In the present study, for AS-TBC500 the delamination is located within the TBC adjacent to the interface and the rough interface is observed (Figs. 3, 5 and 8), compared with PL-TBC200 and PL-TBC500 which showed that the delamination located at the TGO/BC and/or TBC/TGO interfaces had a flat interface. This suggests that the bending effect of the TGO/TBC bilayer is diminished and that the zone subject to friction is large for AS-TBC500, compared with PL-TBC500. Thus, larger frictional contribution for AS-TBC500 than for PL-TBC500 was expected along the wake of the delaminations because the rough interface for the former resulted in larger frictional resistance compared with the latter.

5. Conclusions

The interface shear mechanical properties of structures consisting of as-sprayed and polished bond coats with 200 μm and 500 μm TBC were evaluated, by using the barb test method. The interface compressive residual stress was measured by Raman spectroscopy. The major results obtained are as follows:

(1) The average interface toughness measured was 84 and 106 J/m^2 for PL-TBC200 and PL-TBC500, respectively. The delamination crack propagated at the TGO/TBC, and/or TGO/BC interfaces.
(2) The average interface toughness measured was 123 J/m^2 for AS-TBC500, and the delamination crack propagated within the TBC layer adjacent to the interface.
(3) The interface toughness was larger for the AS-TBC500 than for the PL-TBC200 and PL-TBC500. This was attributed to larger interface residual compressive stress and larger frictional effect for the former than for the latter.

Acknowledgment

This work was partially supported by the New Energy and Industrial Technology Development Organization (NEDO) under the “Nano-Coating Project.”

References

1. Peters, M., Leyens, C., Schulz, U. and Kaysser, W. A., EB-PVD thermal barrier coatings for aeroengines and gas turbines. *Adv. Eng. Mater.*, 2001, **3**(4), 193–204.
2. Padture, N. P., Gell, M. and Jordan, E. H., Thermal barrier coatings for gas-turbine engine applications. *Science*, 2002, **296**, 280–284.
3. Beele, W., Marijnissen, G. and van Lieshout, A., The evolution of thermal barrier coatings-status and upcoming solutions for today’s key issues. *Surf. Coat. Technol.*, 1999, **120–121**, 61–67.
4. Janos, B. Z., Lugscheider, E. and Remer, P., Effect of thermal aging on the erosion resistance of air plasma sprayed zirconia thermal barrier coating. *Surf. Coat. Technol.*, 1999, **113**, 278–285.
5. Tzimas, E., Mullejans, H., Peteves, S. D., Bressers, J. and Stamm, W., Failure of thermal barrier coating systems under cyclic thermomechanical loading. *Acta Mater.*, 2000, **48**, 4699–4707.
6. Preauchat, B. and Drawin, S., Isothermal and cycling properties of zirconia-based thermal barrier coating deposited by PECVD. *Surf. Coat. Technol.*, 2001, **146/147**, 94–101.
7. Kim, G. M., Yanar, N. M., Hewitt, E. N., Pettit, F. S. and Meier, G. H., The effect of the type of thermal exposure on the durability of thermal barrier coatings. *Scripta Mater.*, 2002, **46**, 489–495.
8. Schlichting, K. W., Padture, N. P., Jordan, E. H. and Gell, M. M., Failure modes in plasma-sprayed thermal barrier coatings. *Mater. Sci. Eng.*, 2003, **A342**, 120–130.
9. Schulz, U., Menzebach, M., Leyens, C. and Yang, Y. Q., Influence of substrate material on oxidation behavior and cyclic lifetime of EB-PVD TBC systems. *Surf. Coat. Technol.*, 2001, **146–147**, 117–123.
10. Mumm, D. R., Evans, A. G. and Spitsberg, I. T., Characterization of a cyclic displacement instability for a thermally growth oxide in a thermal barrier system. *Acta Mater.*, 2001, **49**, 2329–2340.
11. Tolpygo, V. K., Clark, D. R. and Murphy, K. S., Oxidation-induced failure of EB-PVD thermal barrier coatings. *Surf. Coat. Technol.*, 2001, **146–147**, 124–131.
12. Guo, S. Q., Mumm, D. R., Karlsson, A. M. and Kagawa, Y., Measurement of interface shear mechanical properties in thermal barrier coating systems by a barb pullout method. *Scripta Mater.*, 2005, **53**, 1043–1048.
13. Tomimatsu, T., Kagawa, Y. and Zhu, S. J., Residual stress distribution in electron beam-physical vapor deposited ZrO_2 thermal barrier coating layer by Raman spectroscopy. *Metall. Mater. Trans. A*, 2003, **34A**, 1739–1741.
14. Portinha, A., Teixeira, V., Carneiro, J., Beghi, M. G., Bottani, C. E., Franco, N. *et al.*, Residual stresses and elastic modulus of thermal barrier coatings graded in porosity. *Surf. Coat. Technol.*, 2004, **188/189**, 120–128.
15. Teixeira, V., Andritschky, M., Fischer, W., Buchkremer, H. P. and Stover, D., Analysis of residual stresses in thermal barrier coatings. *J. Mater. Process. Technol.*, 1999, **92–93**, 209–216.
16. Evans, A. G., He, M. Y. and Hutchinson, J. W., Mechanics-based scaling laws for the durability of thermal barrier coatings. *Prog. Mater. Sci.*, 2001, **46**, 249–271.
17. Vasinonta, A. and Beuth, J. L., Measurement of interfacial toughness in thermal barrier coating systems by indentation. *Eng. Fracture Mech.*, 2001, **68**, 843–860.
18. Mumm, D. R. and Evans, A. G., On the role of imperfections in the failure of a thermal barrier coating made by electron beam deposition. *Acta Mater.*, 2000, **48**, 1815–1827.
19. Clyne, T. W. and Gill, S. C., Residual stresses in thermal spray coatings and their effect on interfacial adhesion: a review of recent work. *J. Therm. Spray. Technol.*, 1996, **5**, 401–418.